Supporting Information

"Halide-mediated modification of magnetism and electronic structure of alpha Co(II) hydroxides. Synthesis, characterization and DFT+U simulations"

Víctor Oestreicher[1,2,†], Diego Hunt[3,†], Ramón Torres-Cavanillas[2], Gonzalo Abellán[2], Damián A. Scherlis[1], Matías Jobbágy[1*]

[1]Departamento de Química Inorgánica, Analítica y Química Física/INQUIMAE, Facultad de Ciencias Exactas y Naturales, Universidad de Buenos Aires, Ciudad Universitaria, Pab. II, Buenos Aires (C1428EHA) Argentina
[2]Instituto de Ciencia Molecular (ICMol), Universidad de Valencia, Catedrático José Betrán 2, 46980, Paterna, Valencia, Spain
[3]Departamento de Fsica de la Materia Condensada, GIyA, CAC-CNEA. Instituto de Nanociencia y Nanotecnología, CNEA-CONICET, San Martin (B1650) Buenos Aires, Argentina

[†]These authors contributed equally to this work.

[*]jobbag@qi.fcen.uba.ar

Experimental results

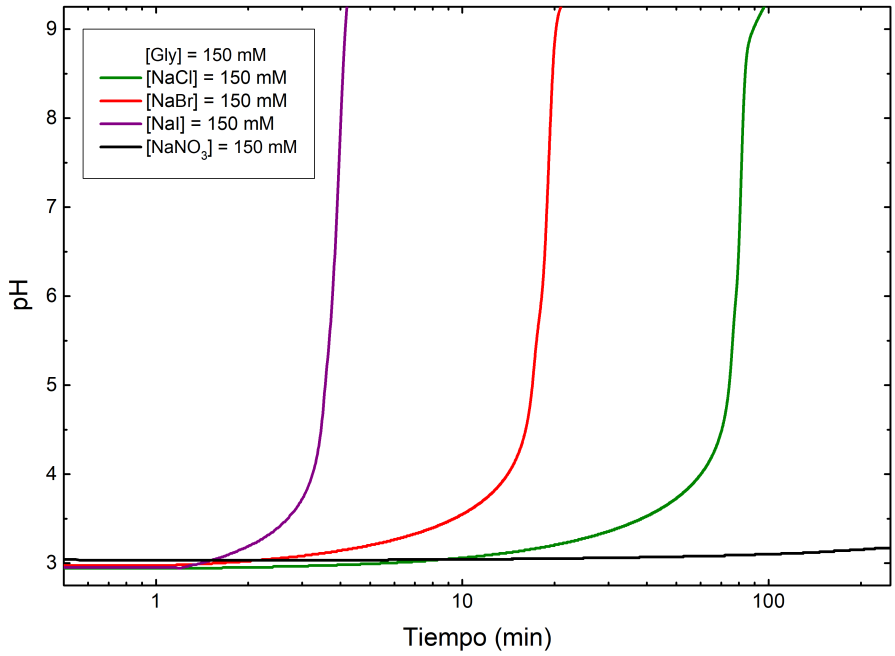

Figure S 1: Evolution of pH at 25 °C of aqueous solutions containing glycidol, halides and nitrate.

Reaction	k $M^{-1}min^{-1}$
$Gly - Cl$	0.63 ± 0.03
$Gly - Br$	2.8 ± 0.5
$Gly - I$	15 ± 1

Table S 1: Alkalinization's rate constants in water at 25 °C for the systems $Gly - Cl$, $Gly - Br$, $Gly - I$ in the concentrations range of $50 - 1000$ mM for Gly and $50 - 150$ mM for NaX.

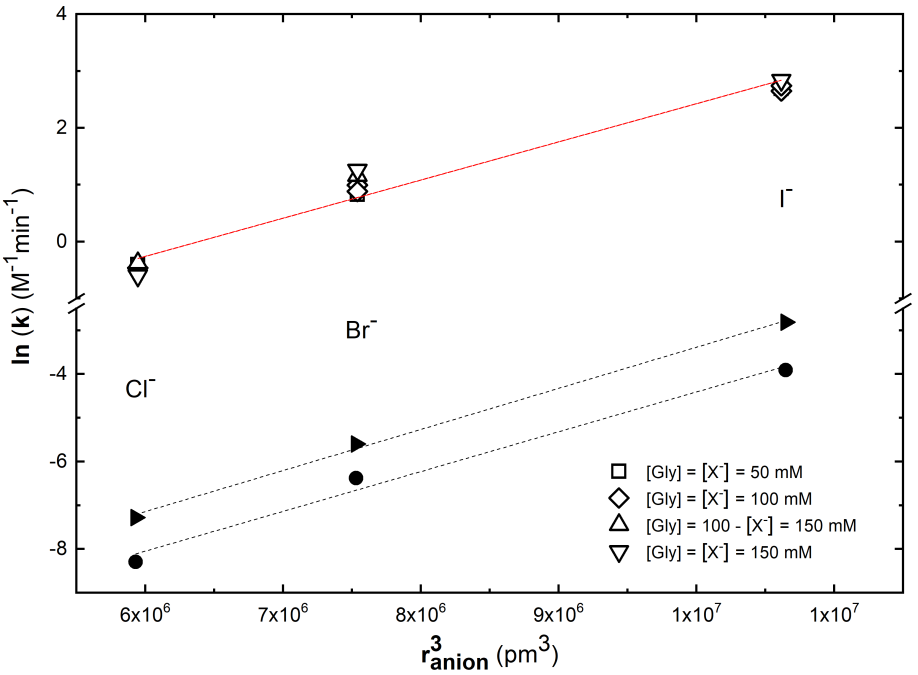

Figure S 2: Natural logarithm of the alkalinization rate constant (k) recorded for glycidol in water at 25 °C as a function of anionic volume (represented by r^3, where r is anionic radii) of the employed halide (nucleophile). The dashed red line represents a linear fit. Results from reference [1] for ethylene oxide (•) and epichlorohydrin (▶) in water at 20 °C, are also presented.

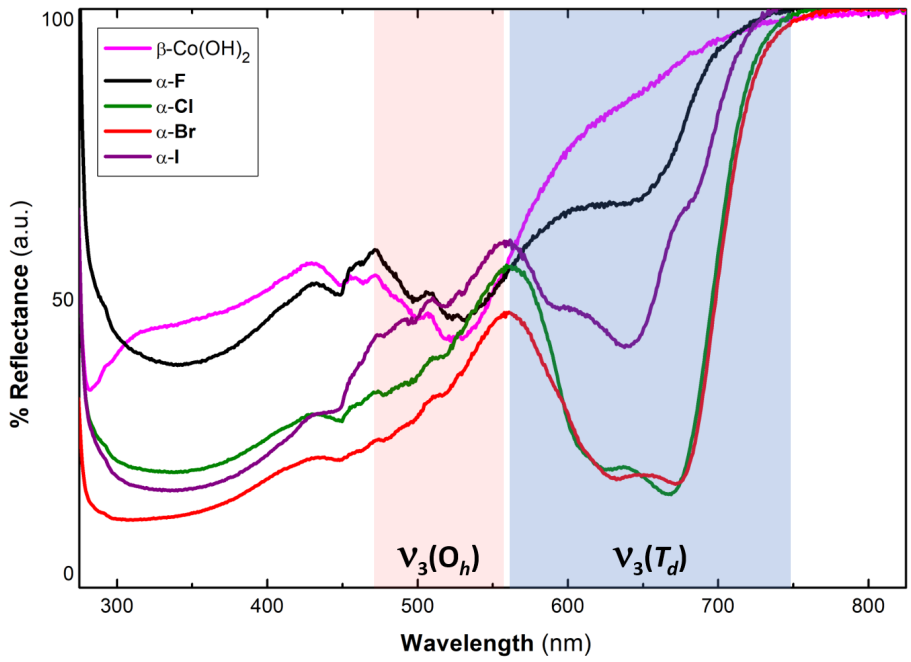

Figure S 3: UV-Vis diffuse reflectance spectra of β-$Co(OH)_2$ and α-X phases. Pink and blue zones indicate the absorption bands associated with the transition energies corresponding to Co(II) octahedral ($\nu_3(O_h)$) and tetrahedral ($\nu_3(T_d)$) coordinations, respectively.

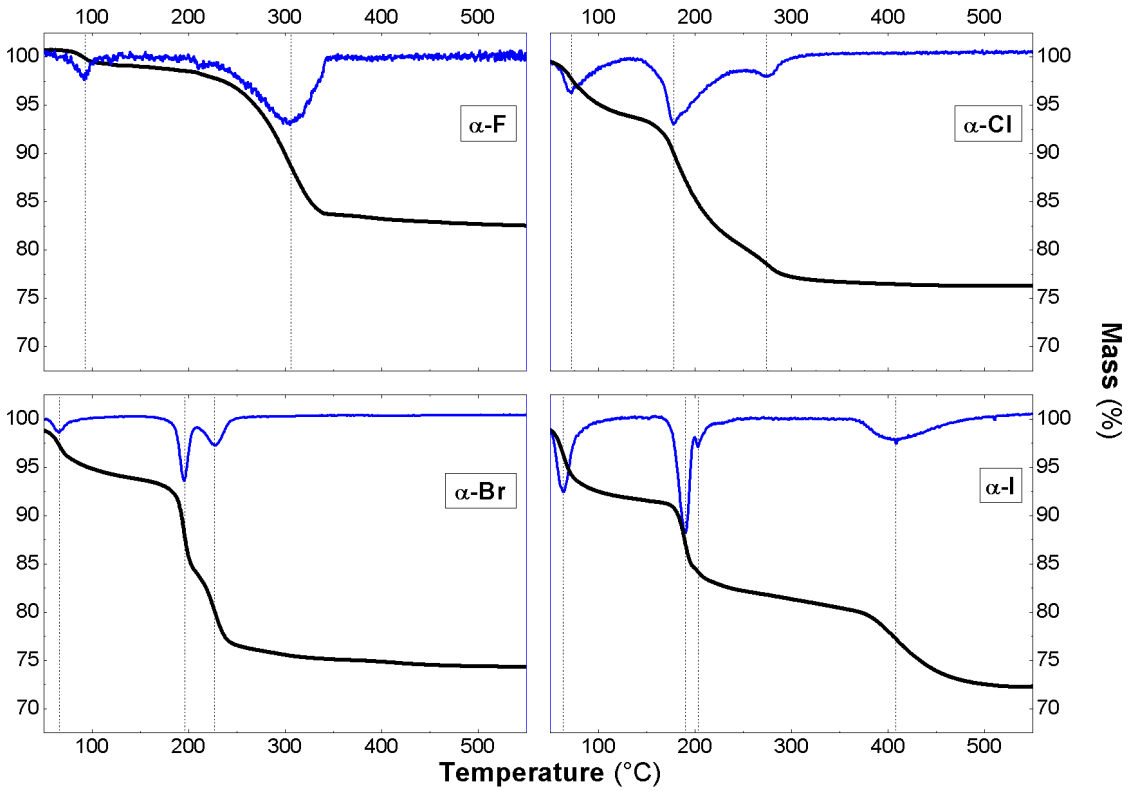

Figure S 4: TGA trace for α-F (upper left panel), α-Cl (upper right panel), α-Br (bottom left panel) and α-I (bottom right panel), decomposed in oxidizing atmosphere at a heating rate of 1 °C/min. The black curves correspond to remmant mass (%) as a function of T, meanwhile the blue lines represent the first derivate of remmant mass (%).

Table S2 compiles the linear fittings for the hydration energy of the solid for different X and n=15. The magnitude of the slope represents the value of ΔE_{ads} per water molecule. These values should be considered only qualitatively and therefore only to show the trends in hydration energies.

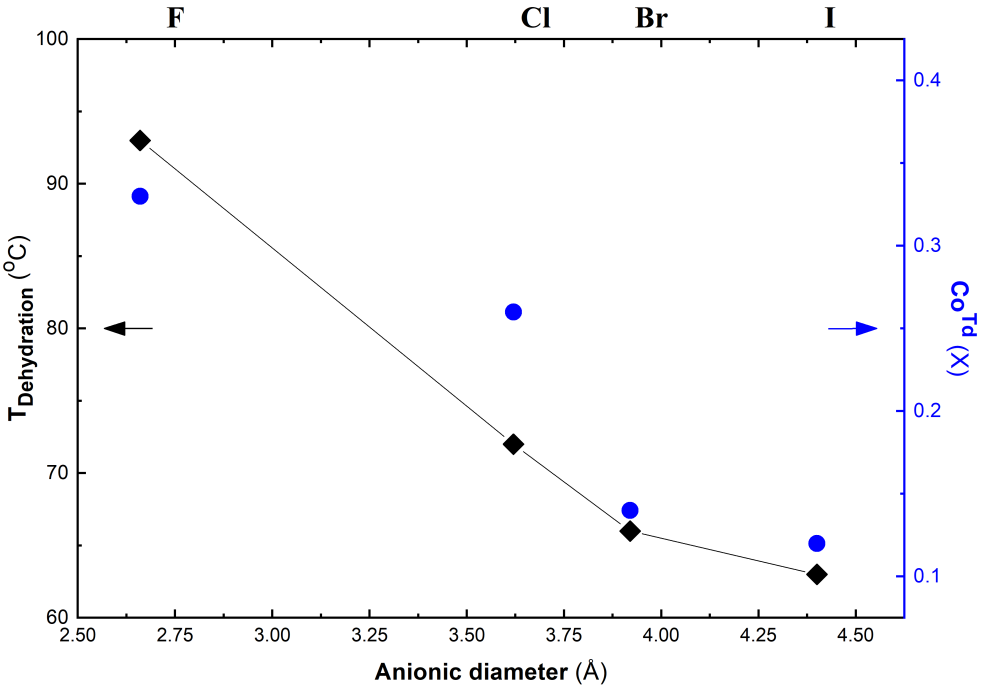

Figure S 5: Dependence of the relative abundance of tetrahedral sites (blue circles) and of the dehydration temperature (black diamonds), both estimated by TGA, on the anionic diameter of the coordinated halide.

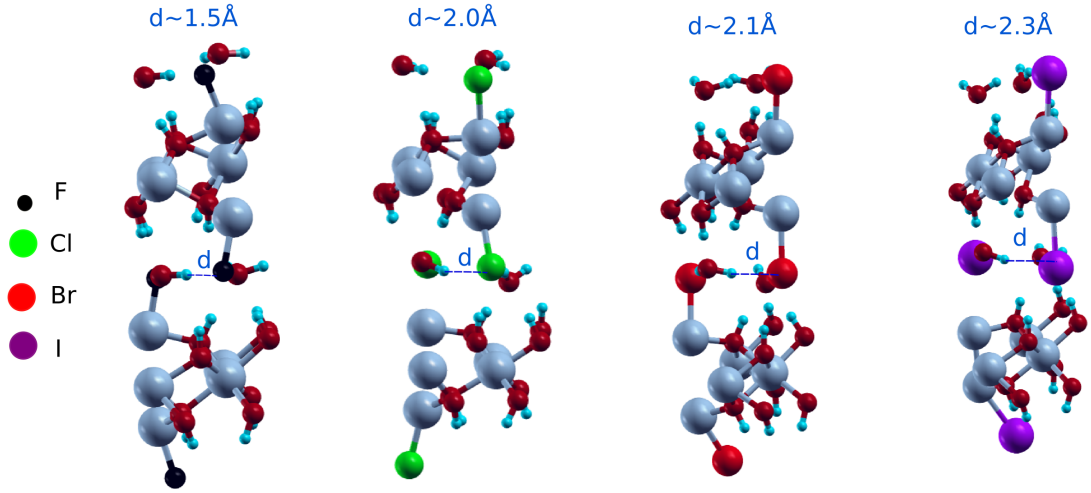

Figure S 6: X-HOH distance (d) for the different $\alpha - \mathrm{X}$ supercell.

X	slope meV/H_2O
F	-2.82
Cl	-2.15
Br	-1.80
I	-1.41

Table S 2: Linear fit of ΔE_{ads} as function of the number of water molecules. The slope represents the value of ΔE_{ads} per water molecule .

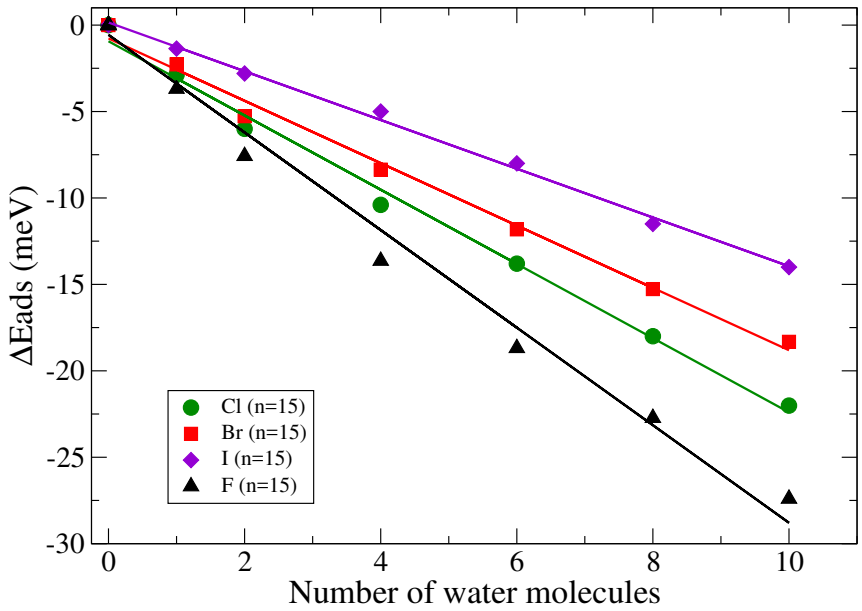

Figure S 7: Computed hydration energies for representative α-X cells as a function of the number of water molecules. Results corresponding to supercells containing two layers. Full lines describe the linear fits.

DFT+U calculations

Table S3 compiles the relative energy of the ferromagnetic (FM) configuration with respect to the antiferromagnetic (AF) ground state, $\Delta E = E_{FM} - E_{AF}$, for different hydroxihalides of varying composition (n). Figure S8 illustrates magnetic states. The ground state is AF for all n values, and the magnitude of the interaction becomes stronger with the radius of halide, and/or with the fraction of tetrahedral sites.

ΔE (meV)				
n	F	Cl[2]	Br	I
3	18	23	25	28
8	8.2	11	12.3	16.1
15	4.5	6	11	13

Table S 3: Relative energies of the FM state in meV ($\Delta E = E_{FM} - E_{AF}$) for the different halides and composition, in a supercell of formula $Co_n^{Oh}Co_2^{Td}(OH)_{2n+2}X_2$.

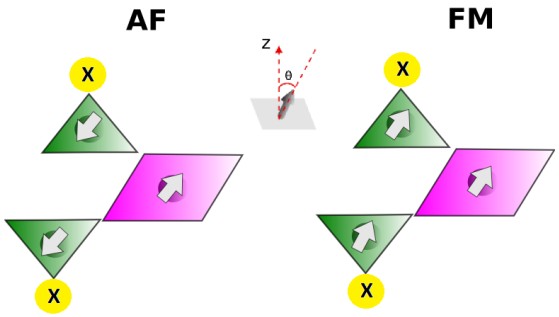

Figure S 8: Schematic representation of the lowest energy accessible magnetic states.

To estimate the magnitude of magnetic interactions, magnetic coupling constants (J_O and J_T in meV) were estimated from the parametrization of an isotropic Heisenberg Hamiltonian with nearest neighbours interactions. The obtained values are compiled in Table S4 and schematic representation of the magnetic coupling interactions is illustrates in the Figure S9

The tendency observed for J_T shows that, for a given value of n, the magnitude of the magnetic interaction between Co^{Td} and Co^{Oh} increases with the size of the anion. These results are consistent with the dominant contribution of the p states of the halide ligands to the valence band in the proximity of the Fermi level, resulting in a more efficient superexchange. The trend observed for J_O is the same as for J_T.

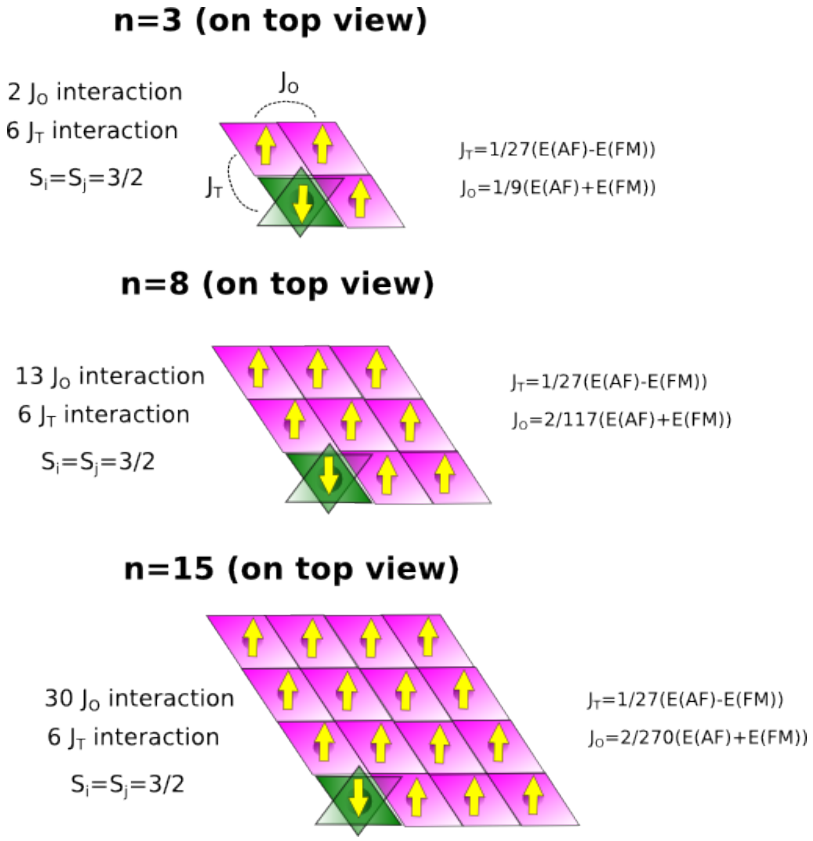

Figure S 9: Schematic representation of the configurations and terms involved in the estimation of the magnetic coupling constants.

	n	J_T	J_O
F	3	-0.67	2
	8	-0.30	0.14
	15	-0.15	0.03
Cl	3	-0.85	2.56
	8	-0.40	0.19
	15	-0.22	0.04
Br	3	-0.93	2.78
	8	-0.46	0.21
	15	-0.45	0.089
I	3	-1.04	3.11
	8	-0.60	0.28
	15	-0.48	0.096

Table S 4: Magnetic coupling constants (meV) for different anions and varying n.

Magnetic characterization

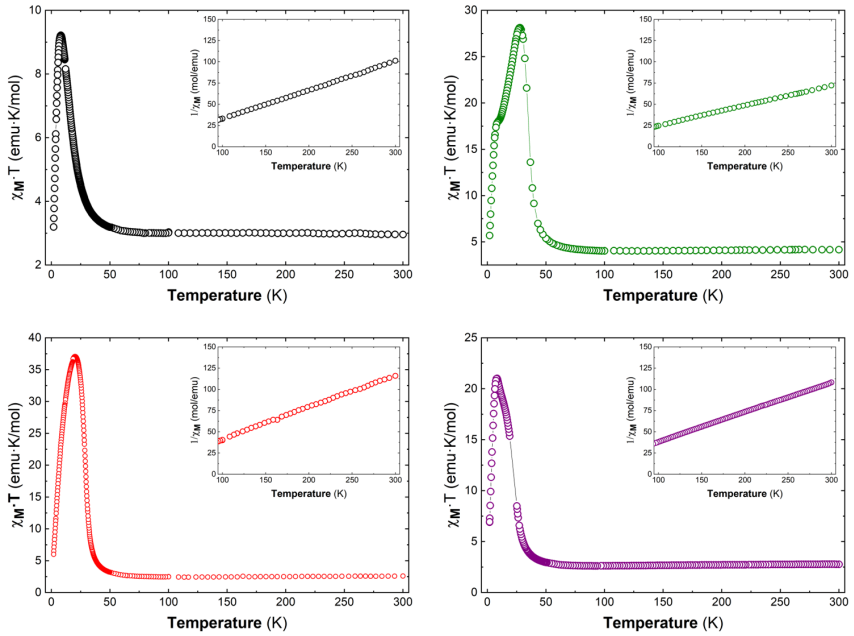

Figure S 10: Magnetic susceptibilities times the temperature values (χ.T) as a function of T for α-X phases: α-F (black), α-Cl (green), α-Br (red) and α-I (purple). Inset: Inverse susceptibility as a function of T.

α-X	M_{sat} (experimental) (μ_B)	M_{sat} (expected) (μ_B)
α-F	1.7	1.0
α-Cl	1.8	1.1
α-Br	1.2	1.3
α-I	1.3	1.3

Table S 5: Experimental and expected saturation magnetization, M_{sat}, for the different α-X.

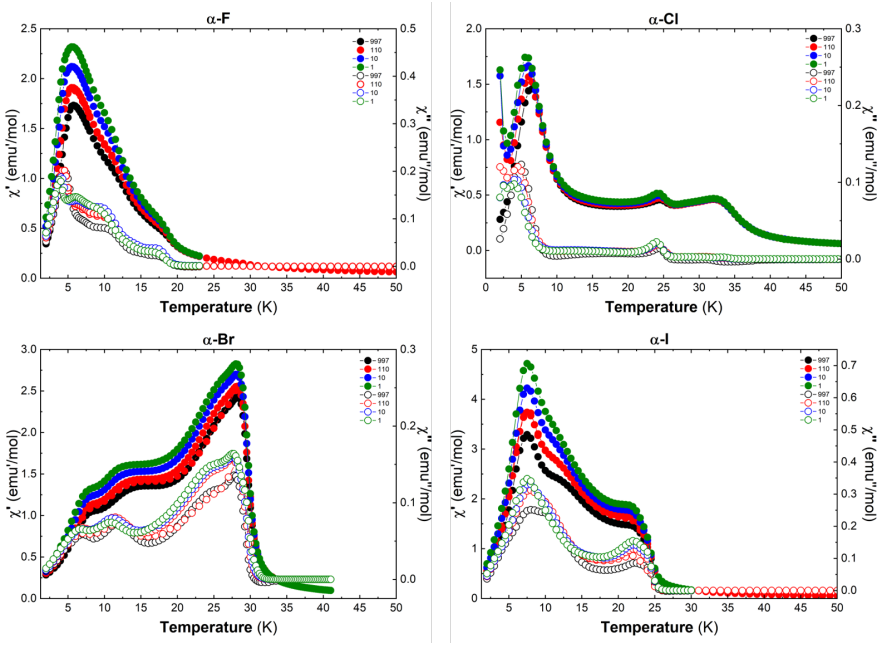

Figure S 11: Dynamic susceptibility for α-X. The real (filled symbols) and imaginary (open symbols) parts of χ are depicted on each plot.

Figure S13 shows the DOS for $\alpha - \mathrm{I}$ with n=8 and n=15; the contribution of the d-states of the octahedral sites becomes more significant as n increases, while the contribution to the valence band of the p-states of the halogen becomes less dominant. Hence, the electronic properties of this family of solids are not evident and result from a complex balance between the contribution of the p-states of the halogen and the d-states of the metallic centers.

α-X	L (cm)	W (cm)	T (cm)
α-F	0.11	0.50	11.10^{-4}
α-Cl	0.15	0.40	40.10^{-4}
α-Br	0.14	0.60	27.10^{-4}
α-I	0.04	0.50	12.10^{-4}

Table S 6: Summary of the L, W and T values for the α-X samples.

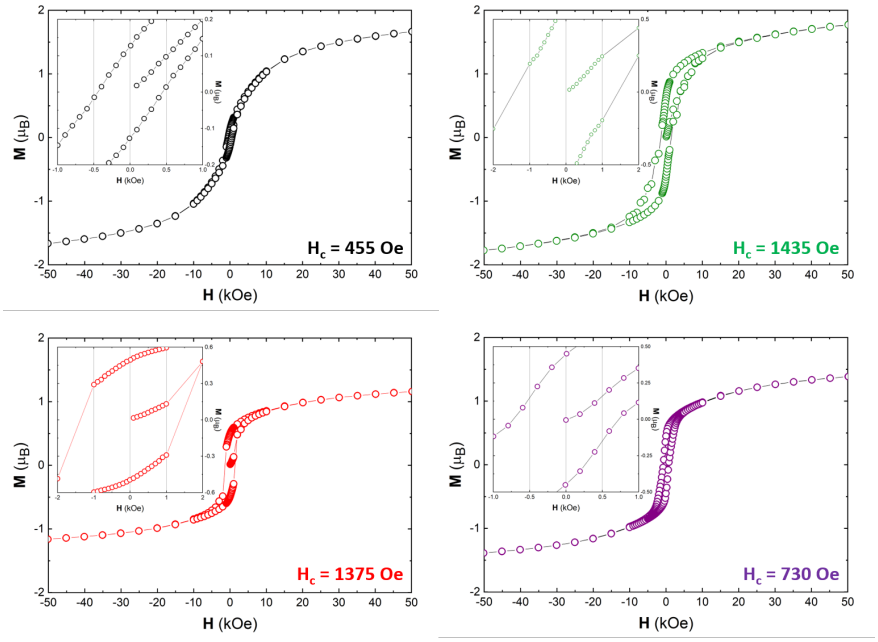

Figure S 12: Isothermal magnetization (2K) for α-X phases: α-F (black), α-Cl (green), α-Br (red) and α-I (purple). The values of coercive field, H_c, are shown in the inserts.

α-X	Conductivity at 400 K (S.cm^{-1})	Activation energy (eV)
α-F	6.10^{-10}	1.55
α-Cl	2.10^{-9}	1.28
α-Br	6.10^{-9}	1.26
α-I	1.10^{-8}	1.08

Table S 7: Summary of the conductivity values obtained at 400 K and the calculated activation energy in the range 370-400 K for α-X samples.

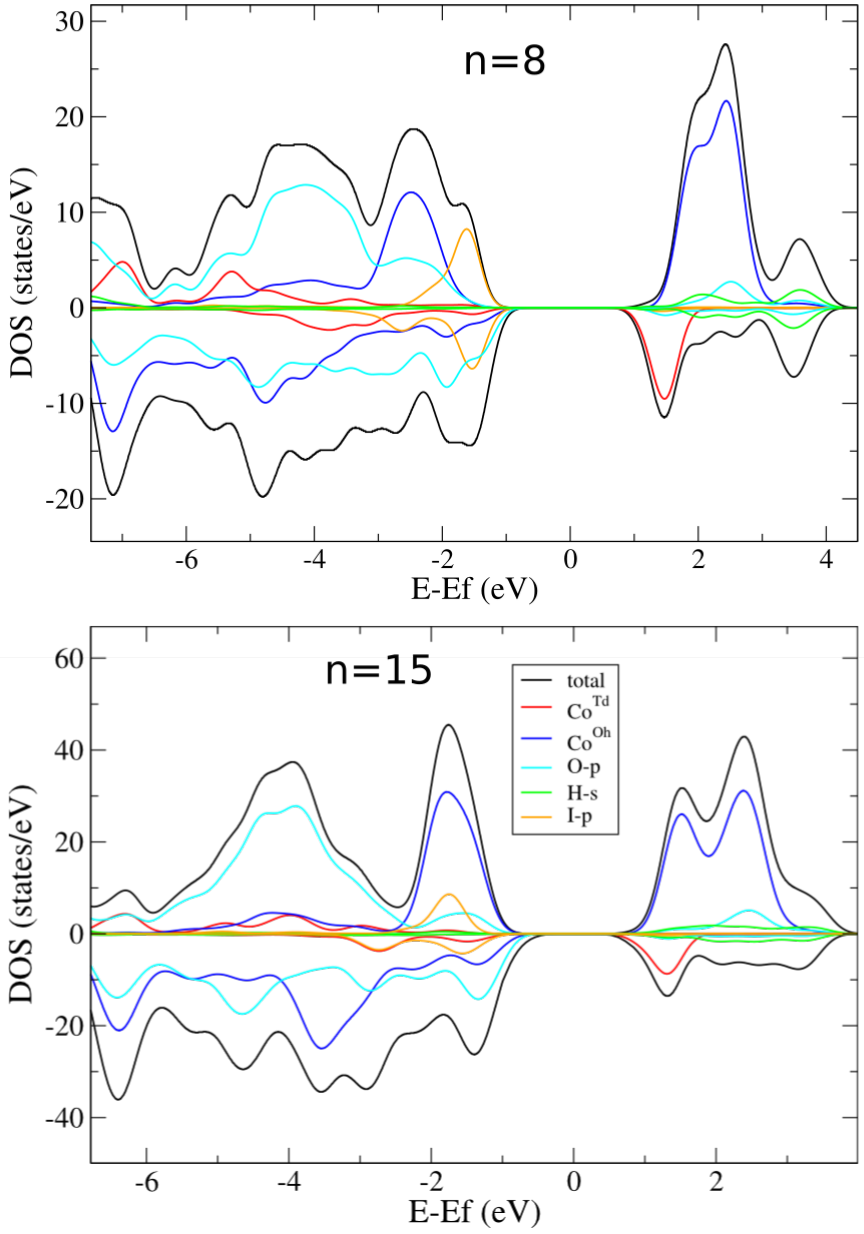

Figure S 13: Density of states for $\alpha - \mathrm{I}$ with n=8 and n=15. The color codes are valid for both panels.

References

(1) Swain, C. G.; Scott, C. B. Quantitative Correlation of Relative Rates. Comparison of Hydroxide Ion with Other Nucleophilic Reagents toward Alkyl Halides, Esters, Epoxides and Acyl Halides. *Journal of the American Chemical Society* **1953**, *75*, 141–147.

(2) Hunt, D.; Jobbágy, M.; Scherlis, D. A. Interplay of Coordination Environment and Magnetic Behavior of Layered Co(II) Hydroxichlorides: A DFT+U Study. *Inorganic Chemistry* **2018**, *57*, 4989–4996.